

Periodic Droplet Formation in Chemically Patterned Microchannels

Olga Kuksenok¹, David Jasnow², Julia Yeomans³, Anna C. Balazs¹

¹ *Department of Chemical Engineering, University of Pittsburgh, Pittsburgh PA 15261*

² *Department of Physics and Astronomy, University of Pittsburgh, Pittsburgh PA 15261 and*

³ *Theoretical Physics, University of Oxford, Keble Road, Oxford, OX1 3NP, U.K.*

Simulations show that when a phase-separated binary AB fluid is driven to flow past chemically patterned substrates in a microchannel, the fluid exhibits unique morphological instabilities. For the pattern studied, these instabilities give rise to the simultaneous, periodic formation of monodisperse droplets of A-in-B and B-in-A. The system bifurcates between time-independent behavior and different types of regular, non-decaying oscillations in the structural characteristics. The surprisingly complex behavior is observed even in the absence of hydrodynamic interactions and arises from the interplay between the fluid flow and patterned substrate, which introduces non-linearity into the dynamical system.

Hydrophilic-hydrophobic patterning is used by a variety of biosystems to direct the motion of fluids at surfaces. For example, hydrophobically-hydrophilically patterned backs help desert beetles to capture water, and hydrophobic patches control water permeation in leaves [1]. This motif is also used to steer the motion and reaction of fluid droplets in liquid microchips [2] and is being utilized to design self-cleaning substrates [1]. Despite the utility of these designs, there have been surprisingly few theoretical studies into the dynamics of fluid flow over chemically patterned surfaces. In this study, we examine a conceptually simple system where two partially miscible fluids, A and B, are mechanically driven (by an imposed shear) to flow past patterned surfaces within a microchannel (see Fig. 1). The system exhibits two distinct steady-states; however, in the transition between the two states, we uncover intricately complicated behavior, where monodisperse droplets of both A-in-B and B-in-A are formed periodically in time (as shown in Fig. 2), and the confined liquid displays regular, non-decaying oscillations in its structural characteristics. Furthermore, we isolate points where this system bifurcates between time-independent behavior and different types of oscillatory patterns. What is striking is that the observed phenomena occur even in the absence of hydrodynamic interaction; this is distinct from well-known instabilities in fluids [3],[4]. Given that the system is relatively simple, the results suggest that complex transitions between well-defined steady-states may well be evident in a broad variety of dynamical systems.

The observed complex oscillatory patterns arise from a competition between advection and thermodynamics as an imposed Poiseuille flow drives the phase-separated fluids to flow over the chemically patterned substrates. As shown in Fig. 1, the top and bottom of the microchannel are decorated with a checkerboard pattern. Each checkerboard is composed of two A(B)-like patches, which are preferentially wetted by the A(B) fluid. The first B patch (in yellow) is placed in the way of the A stream (in blue) and correspondingly, the first A patch is located in the path of the B fluid.

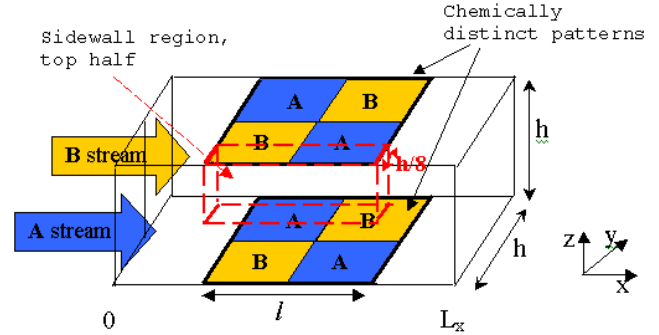


FIG. 1: Schematic of system

The binary fluid is characterized by the order parameter $\varphi(r, t) = \rho_A(r, t) - \rho_B(r, t)$, where $\rho_i(r, t)$ represents the local number density of the i -th component, $i = A, B$. The thermodynamic behavior of the system is governed by the coarse-grained free energy functional, $F = F_0 + \Psi_s$, where F_0 is the Ginzburg-Landau free energy for a binary mixture

$$F_0 = \int d\vec{r} \left[-\frac{a}{2}\varphi^2 + \frac{b}{4}\varphi^4 + \frac{k}{2}|\vec{\nabla}\varphi|^2 \right] \quad (1)$$

and a and b are positive constants. We consider the fluid to be in the two-phase coexistence regime where the equilibrium order parameter for the A(B) phase is $\varphi_{A/B} = \pm\sqrt{a/b}$. The term $\frac{k}{2}|\vec{\nabla}\varphi|^2$ represents the cost of order parameter gradients. The free energy Ψ_s describes the interaction of a fluid element at a point \vec{r} with the patterned substrate. Specifically, we take [5]

$$\Psi_s = \int d\vec{r} \int d\vec{s} \left(\frac{1}{2} V(\vec{s}) \cdot e^{-|\vec{r}-\vec{s}|/r_0} (\varphi(\vec{r}) - \tilde{\varphi}(\vec{s}))^2 \right), \quad (2)$$

where the inner integral represents integration over the substrates. $V(\vec{s}) = V = \text{const}$ on the patterns and is zero otherwise [6], and r_0 represents the range of the substrate potential. We choose $\tilde{\varphi}(\vec{s}) = \varphi_{A(B)}$ to introduce

$A(B)$ -wetted patches at specific regions of the substrate. Through eq (2), the free energy F is reduced when the fluid is $A(B)$ -rich near $A(B)$ -like patches. The evolu-

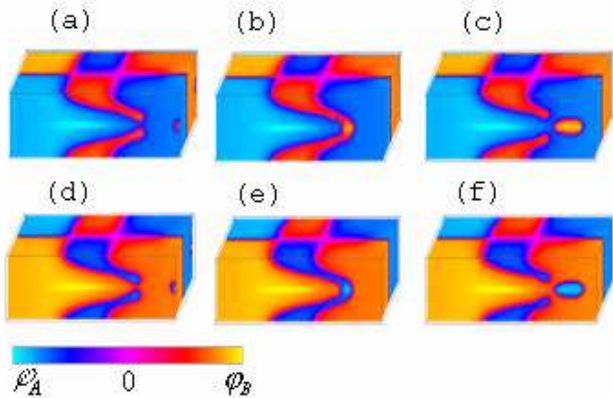


FIG. 2: Periodic droplet formation. Blue represents A-rich and yellow represents B-rich domains. Panels a-c show the "front" and panels d-f show the "back" of the channel, with droplets of B -in- A and A -in- B , respectively. a, d) $t = 31200$, b, e) $t = 32000$, c, f) $t = 33600$. The other parameters are: $H = 3 \cdot 10^{-4}$, $l = 60$, $h = 40$, $r_0 = 5$, $V = 0.003$

tion of the order parameter for this system is described by the Cahn-Hilliard equation, in which the flux of φ is proportional to the gradient of the chemical potential, $J_\varphi = M \vec{\nabla} \mu$, where $\mu = \frac{\delta F}{\delta \varphi}$ and M is the mobility of the order parameter. The imposed Poiseuille flow advects variations in φ along the microchannel. In dimensionless units [7]

$$\frac{\partial \varphi}{\partial t} + \vec{v} \cdot \vec{\nabla} \varphi = \nabla^2 \mu \quad (3)$$

where the length scale is chosen to be equal to the thickness of the interface between A and B fluids, $\xi_{int} = \sqrt{k/a}$, and the scale of time is the diffusion time through that interface, $\tau = \xi_{int}^2/aM$ [7]. The velocity field \vec{v} obeys the Navier-Stokes equation in the over-damped limit, which is appropriate for low Reynolds number flow,

$$0 = -\vec{\nabla} p + \nabla^2 \vec{v} + \vec{H} + C \frac{\delta F}{\delta \varphi} \vec{\nabla} \varphi \quad (4)$$

where p is a Lagrange multiplier that guarantees the incompressibility condition, $\vec{\nabla} \cdot \vec{v} = 0$, and $H_x = (P_{in} - P_{out}) \xi_{int} \tau \eta / L$ is the dimensionless form of the imposed pressure drop ($P_{in} - P_{out}$) along the channel of length L . Because the pressure gradient is applied along the x -axis, only the x -component of the vector \vec{H} is non-zero, $H_x \equiv H$. The last term in eq. 4 is the non-dissipative part of the stress tensor [8] (for the above dimensionless form see [7]); this term represents hydrodynamic interactions. The constant $C = \sigma \cdot \xi_{int} / (a \cdot \eta \cdot M)$ depends on the fluid properties, such as the shear viscosity, η , interfacial tension, $\sigma \approx k \varphi_{eq}^2 / \xi_{int}$, and diffusivity aM . The

value of C determines the importance of hydrodynamic interactions for the specific fluid. For a fluid with a high viscosity, where $C \ll 1$, hydrodynamic interactions can be neglected. In this work, we set $C = 0$; therefore, the velocity profile in our system is determined by the imposed pressure gradient. Thus, advection in a shear flow and diffusion of the fluids to the more wettable A or B domains control the evolution of the order parameter in the system and are responsible for the observed rich behavior [9].

Equations (1)-(3) are discretized and solved numerically by a cell dynamic system method [10] on a $120 \times 40 \times 40$ grid. The following boundary conditions on the walls of the channel are imposed: $\frac{\partial \mu}{\partial n} \Big|_{wall} = 0$, $\frac{\partial \varphi}{\partial y} \Big|_{y=0,h} = 0$ and $\frac{\partial \varphi(\vec{s})}{\partial z} \Big|_{z=0,h} = k^{-1} \int d\vec{s}_i [V(\vec{s}_i) (\varphi(\vec{r}) - \tilde{\varphi}(\vec{s}_i))] \Big|_{\vec{r} \rightarrow \vec{s}_i}$. The last condition arises explicitly from the minimization of free energy in the presence of the substrate potential. At the entry of the channel, we have two-stream flow; at the exit, we assume free draining flow, i.e., $\frac{\partial \varphi}{\partial x} \Big|_{x=L} = 0$. For the velocity field, we assume no-slip boundary condition on the walls [11].

We consider the order parameter evolution in the channel at different values of H . At low H (low velocities), local thermodynamics dominate, and the fluid just mimics the underlying checkerboard pattern, with small distortions in φ caused by the imposed flow. Higher velocities lead to more dramatic changes in φ and yield the complex interfaces between the A/B fluids shown in Figures 2 and 3. This behavior occurs when the scale of spatial distortions in φ within the center of the channel (where the Poiseuille flow exhibits the maximum velocity, v^{max}) is comparable to the length of the patch, i.e., when $v^{max} t_{diff}^l \approx l$, where $t_{diff}^l \approx l^2$ is the characteristic diffusion time over the patch length l . This estimate yields a value of $H \approx 10^{-4}$. For higher values of H , the fluid flows through the middle of the channel with essentially no distortion, while near the top and the bottom substrates, $\varphi(r, t)$ is governed by the patches' wetting properties (see Fig. 3e).

For the intermediate H values, a competition between the preferential wetting interactions and the imposed flow leads to fascinating behavior. On one hand, the wetting effects cause the fluids to diffuse to the respective patches to minimize the free energy and there is the general tendency to minimize interfacial regions between the A and B phases. On the other hand, the imposed flow carries fluid away from the favorable patches. If both substrates contained just the first half of the checkerboard (a single A and B patch), these patches would simply "switch" the location of the fluids, and the imposed flow would move the switched fluids along the channel. The presence of the second set of patches interrupts this flow because both the A and B streams again confront incompatible domains. In three dimensions, each component can avoid

the second unfavorable region by diffusing into the bulk. However, recall that the first yellow (B) patch is on the blue (A) side (see Fig. 2). Thus, the B fluid can extend only so far into the incompatible domain (similar arguments hold for the A fluid). Each fluid forms “arms” that reach from the top and bottom of the walls; these arms can join and pinch off to form a bubble. Our coarse-grained modeling allows such a topology change without any *ad hoc* rules. Figures 2a-c show the order parameter distribution at the “front” of the microchannel; the same behavior occurs for the A fluid at the “back” of the channel (Figs. 2d-f).

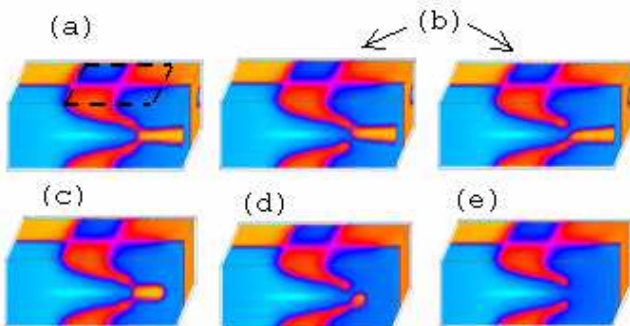


FIG. 3: Order parameter distribution at steady state for different H : a) $H = 2.6 \cdot 10^{-4}$, b) $H = 2.7 \cdot 10^{-4}$, c) $H = 2.79 \cdot 10^{-4}$, d) $H = 3.2 \cdot 10^{-4}$, e) $H = 3.44 \cdot 10^{-4}$. All other parameters are the same as in Fig 2.

Between the limiting cases in Figures 3a and e for relatively low and high H , respectively, three different types of behavior have been observed: two types of periodic behavior and a time-independent state asymmetric with respect to the top and bottom substrates (Fig. 3b); which of the two morphologies shown in Fig. 3b is actually realized for fixed H depends on the noise in the system [6]. The periodic cases exhibit “symmetric” (Fig. 3c) and “asymmetric” oscillations (Fig. 3d). The arms in the figures and all the periodic behavior develop mainly near the sidewalls. In the middle of the box, the Pouseuille velocity field has a maximum and advection prevails. Near the wall, however, the velocity is much smaller and diffusion dominates, allowing the arms to move upward (downward) and join.

To analyze the complex dynamics, we define a parameter that characterizes the integrated changes in $\varphi(\vec{r}, t)$ near the sidewalls:

$$B_i(t) = \frac{1}{V_i} \int d\vec{r} |\varphi(\vec{r}, t) - \varphi(\vec{r}, 0)|, \quad (5)$$

here $i = top, bot$ indicates whether we integrate over the top (see red dashed box in Fig.1) or bottom half of the sidewall region of volume V_i . (We choose the thickness of this region as $h/8$.)

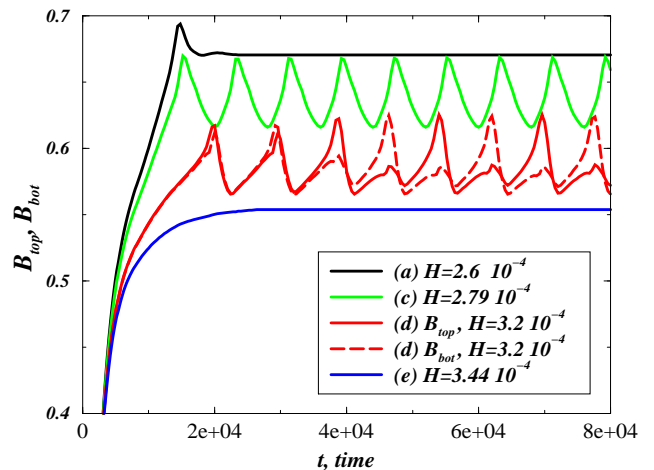


FIG. 4: Evolution of B_{top} and B_{bot} for cases shown in Fig 3, a, c, d and e

The evolution of $B_{top}(t)$ and $B_{bot}(t)$ for different values of H is shown in Fig. 4. Note that $B_{top}(t) = B_{bot}(t)$ for all the symmetric cases (Figs. 3 a, c and e). A case of asymmetric oscillations, where $B_{top}(t) \neq B_{bot}(t)$, is plotted in red. The maxima in the curves correspond to the largest distortions (where the bubbles are biggest); the minima correspond to the structure where the arms are separated by the greatest distance. The two curves for the asymmetric case (Fig. 3d) are similar to each other, but there is a phase shift between them. Each of these red curves displays two maxima and two minima in the periodic state. At early times, the system’s behavior is similar to the symmetric case, but at some time, spontaneous symmetry-breaking occurs. The length of time before steady-state is reached in the asymmetric case depends on degree of noise introduced in the strength of fluid-substrate interaction [6]. The fact that one of the peaks becomes weaker than the other indicates that instead of the arms growing equally from both substrates and simultaneously forming a bubble in the middle, the top arm, for example, grows faster and contributes more to the bubble (higher maximum) than the bottom arm (smaller maximum). But for the next bubble, the situation is reversed, so the whole period encompasses both maxima; this period is roughly twice that of the symmetric case.

We also examined the system response as we change H dynamically. For each value of H , the steady-state value of B_i , or the maximum and minimum in the oscillatory regimes, are shown on the bifurcation diagram in Fig. 5. By abruptly increasing H from below H_1 to above H_6 , the system switches from the symmetric time-independent low-velocity regime (as in Fig. 3a) to the time-independent high-velocity regime (as in Fig. 3e). Correspondingly, by abruptly decreasing H from above H_6 to below H_1 , the system switches from the Fig. 3e

to the Fig. 3a regime. But the transition region between these two points is highly complicated, and incorporates complex bifurcations between all the different states. For $H_1 \leq H \leq H_6$, the behavior of the system depends on the starting value of H , the direction of change (increasing or decreasing) and the magnitude of the change. For example, as we gradually increase H from below H_1 (see red curve in Fig 5), the time-independent symmetric behavior (as in Fig. 3a) becomes unstable and symmetry breaking occurs at the bifurcation point H_1 , giving rise to the one of the two possible time-independent asymmetric types of patterns (as in Fig. 3b). Once the symmetry of the system is broken, we find that it is no longer possible to form arms that grow symmetrically from the top and bottom substrate and subsequently form bubbles that are symmetric with respect to top/bottom. Further gradual increases in H lead to the asymmetric oscillations (as in Fig. 3d) for $H > H_5$. For $H_5 < H < H_6$, we only observe asymmetric oscillations, independent of the direction of change in H . Inside the parameter region $H_2 < H < H_5$, we can observe all the different types of behavior shown in Figs. 3b-d. Gradually decreasing H leads to a transition from asymmetric to symmetric oscillations, and then to the time independent asymmetric state (blue curve) [12]. Figure 5 clearly shows that the system displays hysteresis.

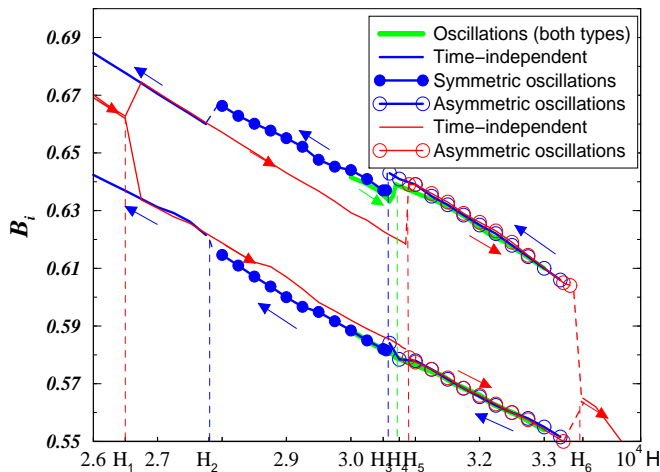


FIG. 5: Bifurcation diagram. Open circles mark asymmetric oscillations, filled circles represent symmetric oscillations, and straight lines indicate time-independent behavior (except green lines that depict both symmetric ($H < H_4$) and asymmetric ($H > H_4$) oscillations). All other parameters (except H) are the same as in Fig 2. In the oscillatory regimes, the top and bottom curves correspond to the maximum and minimum of B_i .

The non-decaying, time-periodic behavior in a simple binary fluid driven through the microchannel arises from interactions between the fluid and the patterned substrate, which introduces non-linearity into the dynamical system. These interactions act as an “activator” in

reaction-diffusion systems [3] and are responsible for the positive feedback. We note that the periods of the oscillations and the positions of the bifurcation points are dependent on the strength of the fluid-substrate interactions and the patch length. Thus, the system dynamics can potentially be controlled by varying these chemical features. In particular, other choices of patterns can potentially lead to new spatiotemporal patterns and dynamical behavior.

Acknowledgements The authors acknowledge helpful discussions with Dr. Sten Ruediger. Supported by the ONR and NSF.

-
- [1] R. Blossey, Nature Materials, **2**, 301 (2003)
 - [2] See for example: H. Gau, S. Herminghaus, P. Lenz and R. Lipowsky Science, **283**, 46 (1999).
 - [3] M.C.Cross, P.C.Hohenberg, Rev.Mod.Phys. **65**, 851 (1993).
 - [4] We note that T. Thorsen *et al* Phys. Rev. Letts.**86**, 4163 (2001) experimentally demonstrated complex pattern formation involving water/oil/surfactant mixtures in microchannels that arises from a well-known competition between interfacial tension and shear forces. In the latter study, interactions between immiscible liquids introduce non-linearity into the system, while in our case, non-linearity is introduced and controlled by the patterned substrate.
 - [5] A.C. Balazs et al., J. Phys. Chem. B, **104**, 3411 (2000)
 - [6] We introduce noise in the strength of the interaction at each point of the checkerboard pattern, i.e. $V(\vec{s}) = V(1 + 0.03\zeta(\vec{s}))$, where the independently distributed random numbers $\zeta(\vec{s})$ lie in $[-1,1]$.
 - [7] D. Jasnow, J.Vinals, Phys.Fluids **8**, 660 (1996)
 - [8] A.J.Bray, Adv. Phys. **43**, 357 (1994).
 - [9] We have, however, carried out simulations with hydrodynamic interactions (where we set $C = 10$). We observed qualitatively similar periodic droplet formation, but the quantitative characteristics (the actual value of the imposed pressure gradient when periodic droplet formation occurs, the period and amplitude of oscillations) were altered by the actual value of C .
 - [10] Y. Oono, S.Puri, Phys.Rev.A, **38**, 434, (1988)
 - [11] H-Y. Chen, D. Jasnow and J.Vinals, Phys. Rev. Letts.**85**, 1686 (2000).
 - [12] The period of the oscillations consists of three characteristic times: τ_1 , for two retracted arms to reach each other, τ_2 , for the diffusive growth of a droplet, and τ_3 , the time during which the droplet moves away from the second patch. The first time, τ_1 , can be estimated as the time for advective motion of the arms along a distance comparable to the patch length (near the sidewall where velocity is very small). Increases in H lead to increases in τ_1 because the distance over which the arms are the most separated is larger for higher H . The time scales τ_2 and τ_3 decrease with H . As a function of H , the period for symmetric oscillations is almost constant, while for asymmetric oscillations, it grows rapidly with increasing H . In the latter case, the arm growth from the substrate (τ_1) provides the main contribution to the total period.